The Relation Between Crystalline Phase, Electronic Structure, and Dielectric Properties in High-K Gate Stacks

S. Sayan[1,3], M. Croft[2], N.V. Nguyen[3], T. Emge[1], J. Ehrstein[3], I. Levin[4], J. Suehle[3], R.A. Bartynski[2], E. Garfunkel[1]

[1]*Department of Chemistry, Rutgers University, Piscataway, NJ 08854*
[2]*Department of Physics and Astronomy, Rutgers University, Piscataway, NJ 08854*
[3]*Semiconductor Electronics Division, National Institute of Standards and Technology, Gaithersburg, MD 20899*
[4]*Ceramics Division, National Institute of Standards and Technology, Gaithersburg, MD 20899*

Abstract. As high permittivity dielectrics approach use in metal-oxide-semiconductor field effect transistor (MOSFET) production, an atomic level understanding of their electronic and dielectric properties is being rigorously examined. In our work we illustrate studies leading to such an understanding for the important materials HfO_2 and ZrO_2. Valence and conduction band densities of states for $HfO_2/SiO_2/Si$ and $ZrO_2/SiO_xN_y/n$-Si structures were determined by soft X-ray photoemission and inverse photoemission. First principles calculations were used to help in assigning valence band maxima and conduction band minima. The energies of defect states at the band edges were determined by comparing the theoretical and experimental results. From this information, we are able to show that both of these dielectric materials have high enough barriers for both electron and hole transfer. We show that the crystal structure in ultrathin ZrO_2 films has considerable effects on permittivity as well as bandgap. The films reported here are predominantly amorphous below a critical thickness (~5.4 nm) and transform to the tetragonal phase upon annealing, while thicker films appear tetragonal as grown. Finally, bandgaps obtained from combined PES and IPES studies were compared with the optical bandgap derived from ellipsometry measurements. The difference in the bandgap values found in this comparison can be attributed to the final state effects in the excitation processes of the spectroscopies involved. We discuss the interplay of the dielectric's crystal phase, defects and electronic properties, as well as the impact of this understanding on possible tailoring of the film phase for improving band-gap, band-offset and leakage. Finally, we note that lack of sufficient understanding of the dielectric's phase and electronic properties can have negative impact on the ability to correctly determine a film's EOT.

Keywords: Band Offsets, Dielectric Band-gap, Hafnium dioxide (HfO_2), High-K dielectrics, MOS Gate Stack, Photoemission, Zirconium Dioxide (ZrO_2)

INTRODUCTION

Future nano-electronic devices will require a switch to high permittivity (high-κ) gate dielectric materials since the use of SiO_2 and SiO_xN_y dielectrics will not be acceptable for many applications due to high tunneling currents. ZrO_2 and HfO_2 are being considered as potential replacements for SiO_2 because of their relatively high dielectric constant, as well as their reasonable thermal stability and moderately large band gaps [1,2].

One of many requirements of potential high-κ dielectric candidates is that both valence and conduction band offsets of the material (with respect to the substrate silicon and gate electrode band edges) should be greater than 1 eV [2]. The current consensus seems to be that the best dielectric will be a multi-component HfO_2-based one (ZrO_2-based ones might be preferred if the thermal budget could be lowered). The band gaps of these materials are smaller than that of SiO_2; hence a good knowledge of their valence and conduction band offsets as well as their measurement and determination is critical.

A variety of factors such as degree of crystallinity, interface roughness, chemical homogeneity, and stoichiometry can have a direct effect on the dielectric properties and leakage currents across such dielectric layers[2]. The permittivity of these two materials in the literature varies from 16 to 45 for HfO_2 and 18 to 35

CP 788, *Characterization and Metrology for ULSI Technology 2005,*
edited by D. G. Seiler, A. C. Diebold, R. McDonald, C. R. Ayre, R. P. Khosla, S. Zollner, and E. M. Secula

for ZrO_2 [3-10]. Similarly, the reported band gap values for these materials are in the range of 5.1 eV to 6.0 eV, with ZrO_2 reported to have a slightly smaller band gap [8,11,12]. One possible reason for the rather large range of values reported in the literature could be that the samples prepared by different methods in various labs have significant microstructural differences. It is therefore important to characterize the microstructure of these materials since the electrical properties of these materials are dependent on their microstructure. There have been many reports on the electrical properties of zirconia films for application as gate dielectrics, but detailed reports on microstructural characterization along with electrical characteristics are scarce [11,13].

The known crystal phases of ZrO_2 and HfO_2 are monoclinic, orthorhombic, cubic, and tetragonal, where the latter three phases are metastable under ordinary temperatures and pressures for bulk films. Film thickness, stress, grain-size, and impurities may lead to the stabilization, or predominance, of one or more of these phases. It is therefore reasonable to observe different electronic and dielectric responses due to differences in thickness of ultrathin films or differences in the sample history (e.g., preparation methods: chemical vapor, atomic layer, or physical vapor deposition).

First principles density functional theory (DFT) calculations on all crystal phases of HfO_2 and ZrO_2 were performed by Zhao and Vanderbilt [14-16]. They have shown that the dielectric response and bandgap of these materials are strongly phase dependent. For example, the permittivity of the tetragonal phase of ZrO_2 was estimated to be almost double that of the monoclinic and amorphous phases. Recently we have also reported experimental observations that the electronic structures (including energy gap, band offsets, charge neutrality level, and permittivity…) of these materials are phase (crystal structure) dependent [13]. One message of this work is that the crystal structure of this class of high-κ dielectrics should be reported along with any experimental data if a valid comparison of results from different experimental techniques is desired. In this review, we experimentally explore the issue of crystal structure in ultrathin films of HfO_2 and ZrO_2 and the effect of crystal structure on dielectric properties and band gap.

The experimental determination of valence band maxima (VBM) and conduction band minima (CBM) remains a controversial issue. The reports of high-κ materials on silicon using photoemission and optical methods usually employ a "straight-line" method where the valence and conduction edges are determined using a linear extrapolation of the data (at the band edges) to the "background" intensity level. Although this particular method does not have a strong physical justification (the band shape is part of the intrinsic nature of the material and is rarely "straight"), it serves as a common method for all in the field to compare their work.

In general, polycrystalline semiconductors present a higher concentration of defects and imperfections than bulk single crystals. The presence of structural disorder can also be related to deviations from ideal stoichiometry and/or impurities. One major consequence is that new electronic states may appear in the band gap that manifest themselves as increased densities of states in the vicinity of the band edges; these are sometimes called band tail states [17]. The presence of band tail states not only reduces the observed gap but it may increase carrier transport across or scattering in or near the dielectric. The defect bands, some formed by the broadening and merging of energy levels, may also overlap with the bands of the perfect crystal [18]. The experimentally observed density of states can be considered as a superposition of the perfect crystal DOS and defect bands. The change in the band edge clearly changes the offset assignments and leads to a reduced "effective gap." To our knowledge, the exact value of an intrinsic energy gap has yet to be determined for an ultrathin dielectric film since all high-κ films reported to date are either polycrystalline or amorphous and have crystal imperfections (defects) which inevitably contribute to the electronic properties. What is needed are careful measurements on bulk single crystals and crystalline ultrathin films to confirm theoretical predictions; a goal yet to be realized for this class of oxides.

States can appear in the gap and can be either structural or compositional in nature (e.g. metal or oxygen vacancy) [19]. The charge neutrality level of these states with respect to the Fermi energy in the system will determine their occupancy and charge, as well as their effect on the band alignment. The rate at which the occupancy of these states change as the electrode voltages are varied, will depend on their distance from the electrode and other defects, as well as their energy, and may be critical in determining device electrical characteristics.

EXPERIMENTAL

HfO_2 films were deposited on 11Å SiO_xN_y/p-Si at ~400 °C using chemical vapor deposition (CVD), with

Hf-tetra-tert-butoxide as the precursor; details of the growth can be found elsewhere [20]. The primary substrate used in the HfO_2 studies reported here was p-type Si(100) with a doping concentration of $\sim 1\times10^{15}$ cm^{-3}. The ZrO_2 films were grown by atomic layer deposition ALD at 300 °C using alternating cycles of $ZrCl_4$ and H_2O; details can be found elsewhere [21]. The substrate used was n-type Si(100) with a doping concentration of $\sim 1\times10^{16}$ cm^{-3}. Some of the samples were annealed in various ambient and temperature regimes including a 500 °C oxidation, a 400 °C forming gas anneal (FGA), 600 °C and 800 °C rapid thermal anneals in nitrogen (RTA/N_2), and an 800 °C vacuum anneal (10^{-9} Torr).

Soft X-ray photoemission measurements were performed at the National Synchrotron Light Source (NSLS) at Brookhaven National Laboratories on the U8B beamline using 120 eV to 400 eV photon energies. The X-ray absorption spectroscopy (XAS) measurements on ZrO_2 thin films were also performed at NSLS on beamline X19A in the total electron yield mode [22]. The inverse photoemission studies were performed in fluorescence mode in the 18 eV to 22 eV electron energy range at Rutgers University. Wide-angle X-ray scattering (WAXS) was performed to obtain XRD-patterns of several ZrO_2 and HfO_2 thin film samples using a Bruker HiStar area detector and an Enraf-Nonius FR571 rotating anode X-ray generator equipped with a graphite monochromator (Cu Kα; λ = 1.5418 Å)*.

Vacuum ultraviolet spectroscopic ellipsometry (VUV-SE) measurements were performed on a commercial instrument with the spectral range from 1.5 eV to 8.5 eV in steps of 0.02 eV. A four-phase model consisting of silicon substrate, SiO_2 interfacial oxide, ZrO_2 film, and air ambient was employed to extract the real and imaginary part of dielectric functions ($\varepsilon = \varepsilon_1 + i\varepsilon_2$) of the ZrO_2 films. The optical interfacial oxide thicknesses are correlated with high resolution transmission electron microscopy (HRTEM) micrographs and included in the four-phase model; the thicknesses reported are the ZrO_2 optical film thickness.

This paper is organized as follows: we first describe the crystal structure analysis of HfO_2 and ZrO_2 films, which enables the selection of the correct theoretical DOS. Then, the method for determination of band edges followed by the band offset description will be presented. The PES and IPES results and final simplified band diagrams will be shown. Finally, we discuss the effect of microstructure on electronic and dielectric properties of ZrO_2 and conclude with final remarks.

XRD Measurements

X-ray diffraction studies were performed on a series of films of different thicknesses (not shown) of HfO_2 and ZrO_2.

HfO_2 – XRD results

The thickness range was 125 Å to 1150 Å, as determined by Rutherford Backscattering Spectroscopy (RBS) assuming a density of 9.68 g/cm^3 for all samples. All twelve of the significant diffraction peaks for the 1150 Å sample were consistent with monoclinic HfO_2. As the thickness is reduced, the crystallinity of the films decreases, as is evident from the broadening of the diffraction peaks, consistent with a decrease in the average scattering domain (Figure 1).

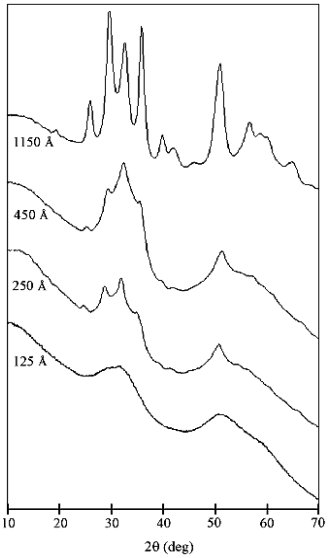

FIGURE 1. X-ray diffraction data for four different HfO_2 layer thicknesses: 125 Å, 250 Å, 450 Å, 1150 Å. Vertical axis – arbitrary units – no label needed.

ZrO_2 – XRD results

A series of as-deposited ZrO_2 films of different thickness was studied by XRD (Figure 2). For the samples with optical thicknesses greater than ≈ 49 Å, only the tetragonal phase could be positively identified

* Certain commercial products are identified here to specify the experimental procedure adequately. Such identification does not imply recommendation or endorsement by NIST nor does it imply that the equipment is necessarily the best available for the purpose.

by XRD; see the feature at 30.3 °. Based upon the decreasing relative intensity and increasing relative peak width of the <101> reflection around 30.3 ° for the tetragonal phase, the degree of crystallinity decreases with decreasing film thickness. The 49 Å as-deposited film was found to be predominantly amorphous. The measurements on thinner samples did not yield any useful information because of insufficient scattering.

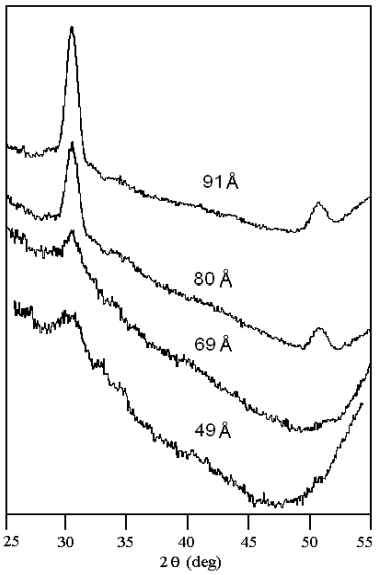

FIGURE 2. X-ray diffraction spectra of ZrO_2 films of optical thickness 49 Å, 69 Å, 80 Å, 91 Å. Vertical axis – arbitrary units – no label needed.

ZrO_2 – XAS Results

XAS studies were also performed on the same thickness series of as-deposited ZrO_2 films, mentioned above, where the approach was to compare the L_2 and L_3 edges of Zr in these films with those of ZrO_2 in known crystal structures. The XAS near edge structure of the L_2 and L_3 edges of Zr compounds is dominated by transitions into unoccupied final Zr-4d states. Although both the L_2 and L_3 edges probe the 4d-DOS, we focus on the L_2 edge here because it involves only $4d_{3/2}$ final states and is less sensitive to multiplet effects [23]. The XAS L_2-edge spectra of a thin, as-deposited ZrO_2 film of 44 Å optical thickness is given in Figure 3. The XAS spectrum of this film is not consistent with that of any pure single phase (i.e., tetragonal, cubic, or monoclinic). The XRD measurements on thin as-deposited samples indicate that these thin, as-deposited films are predominantly amorphous. The spectrum obtained for as-deposited thicker films (e.g., the 71 Å film in Figure 3) is consistent with that of the tetragonal phase, indicating that, as the films get thicker, the tetragonal structure becomes favored over an amorphous one. An important point to be emphasized here is that the peak splittings and relative intensity apparent in the Zr-L_2 edge measurements provide a convenient tool for identifying the structural changes in these ZrO_2 films.

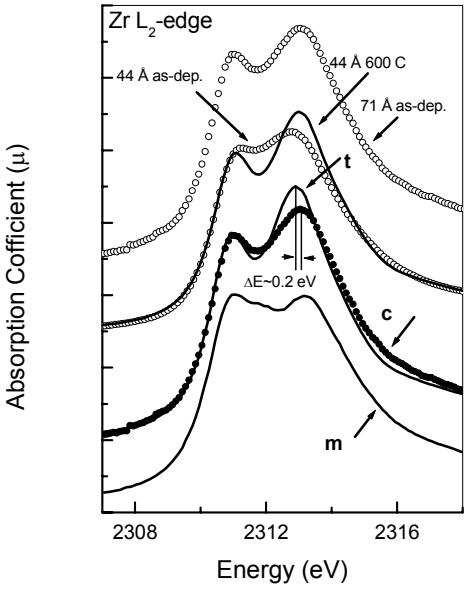

FIGURE 3. Zr-L_2-edge XAS spectra of: bulk monoclinic (m) and yttrium stabilized cubic (c) phases of zirconia, and a representative film spectrum of tetragonal (t) ZrO_2 (confirmed by XRD), representative spectra of amorphous ZrO_2 films before and after annealing. The distinct spectral changes associated with the tetragonal phase, induced by annealing (44 Å RTA 600°C spectrum) or increased film thickness (71 Å as-deposited) should be noted.

Method for determination of band edges

Zhao and Vanderbilt have performed first principles DFT calculations on all crystal phases of HfO_2 and ZrO_2, including the structural and dielectric properties of amorphous ZrO_2. Details of these calculations can be found elsewhere [14,24]. Although the band gap is not calculated exactly in this method, the shapes and densities of state of the occupied and unoccupied bands are thought to be accurate. Since the crystal structure of the HfO_2 and ZrO_2 films studied here were determined to be predominantly monoclinic, and amorphous respectively, only the theoretical density of states for monoclinic HfO_2 and amorphous ZrO_2 are considered.

In order to determine a more accurate energy gap as well as the valence band maximum, (VBM), and conduction band minimum, (CBM), positions, we have employed the following procedure which combines experimental and theoretical results. First, the theoretical density of states for monoclinic HfO_2 (amorphous ZrO_2) is convoluted with the appropriate spectrometer response functions for both PES and IPES spectra. This is accomplished by modeling the region in the vicinity of the Fermi level by a step function and a Gaussian function whose width represents the experimental spectrometer response function. The height of the first main peak below (above) the VBM (CBM) is normalized (such that the experimental and theoretical heights are the same). Then. the broadened theoretical curves in the band edge region are shifted until they align with the experimental curves. Details of this procedure can be found in reference 27. The energy shifts needed to align the experimental (PES and IPES) and theoretical densities of states are added to the theoretical gap to obtain a new effective band gap. The energy separation ($\Delta E_{CBM} = E_{CBM} - E_f$ and $\Delta E_{VBM} = E_{VBM} - E_f$) between the Fermi level and VBM and CBM are then calculated.

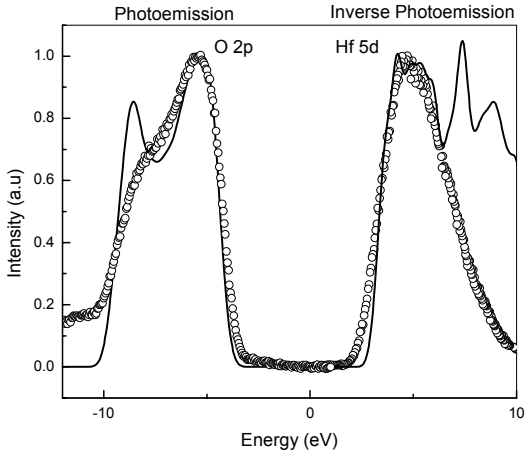

FIGURE 4. Combined photoemission and inverse photoemission spectra of a 28 Å HfO_2/SiO_xN_y/p-Si gate stack along with convoluted DOS for monoclinic HfO_2.

Determination of band offsets

In order to extract the valence and conduction band offsets, a knowledge of the position of the Fermi level within the silicon bandgap is required. The position of the Fermi level with respect to the CBM and VBM of Si can be calculated from the doping density and conductivity type of the silicon substrate using standard methods [25,26]. To obtain the Si-HfO_2 (Si-ZrO_2) offsets, the energy separation between the Fermi level and CBM of Si is subtracted from the position of the CBM of HfO_2 (ZrO_2) with respect to the Fermi level (using our combined experimental-theoretical method).

PES and IPES Measurements Results

HfO_2

The combined photoemission and inverse photoemission data obtained from a 28 Å HfO_2/SiO_xN_y/p-Si, as well as the theoretical densities of state for the valence and conduction bands are shown in Figure 4. The valence band mainly consists of O 2p-like non-bonding orbitals of π-symmetry while the conduction band is mainly Hf 5d-like non-bonding orbitals. All energies are referenced to the Fermi level which is determined by a clean polycrystalline gold or platinum sample. Special care is taken when determining the spectrometer response functions for both IPES and PES. The energy shifts needed to align the experimental (PES and IPES) and theoretical densities of states are added to the theoretical gap to obtain a band gap of 6.70 eV. The energy separations ($\Delta E_{CBM} = E_{CBM} - E_f$ and $\Delta E_{VBM} = E_{VBM} - E_f$) between the Fermi level and the valence band maximum, VBM, and conduction band minimum, CBM, are found to be 3.87 eV and 2.83 eV respectively. Uncertainties for energies extracted from photoemission and inverse photoemission measurements are estimated to be about 0.1 eV. Good agreement is observed between the experimental and theoretical valence band densities of states (specifically, the band widths and main features), even though the theoretical density of states is not modified for photoemission cross-sections (transition matrix elements). However, one would expect that the photoelectron cross-section across the band would be similar (if not the same) since the valence band is almost exclusively made up of oxygen 2p-like orbitals of σ and π-symmetries. In the case of the unoccupied conduction band, the overall width of the band and the first two features agree reasonably well with theory. However the intensity in the higher energy region of the conduction band clearly does not agree well. It is important to note the observed excess density of states near the band edges for reasons that will be discussed in the following sections.

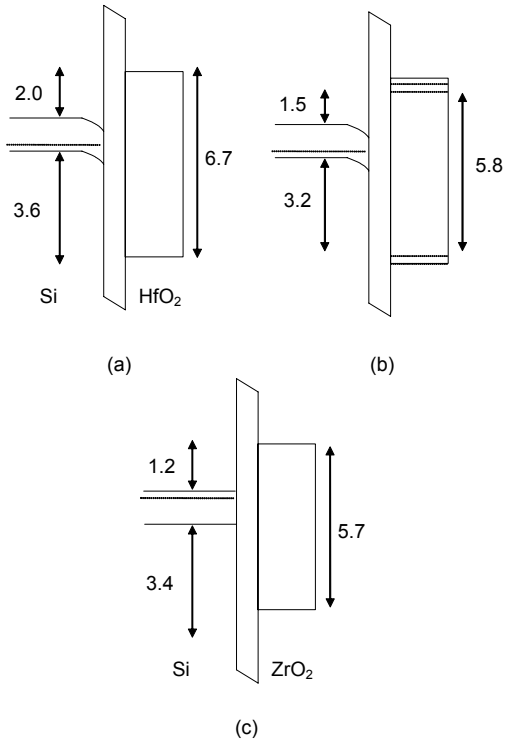

FIGURE 5. Simplified energy band diagram of HfO_2/SiO_xN_y/p-Si gate stack (a) intrinsic (b) including band-tail states, (c) ZrO_2/SiO_xN_y/n-Si.

Figure 5 shows simplified energy band diagrams for this gate stack (for both cases: intrinsic and with band tail states). The valence and conduction band offsets are found to be 3.61 eV and 1.97 eV, respectively. These offsets are large enough to confirm HfO_2 to be a viable high-κ candidate from a barrier height perspective. However, in order to be able to compare the values with results found by others, one must remember to specify the phase of the HfO_2 as well as the method of edge or gap determination. An additional property of the dielectric material, the electron affinity (EA), can also be determined. Since both the electron affinity of silicon (4.15 eV) and the conduction band offset are known, the electron affinity of HfO_2 can be extracted as 2.18 eV (Table 1). When the straight line method was used to determine the offset, we obtained 3.28 eV and 1.46 eV for the valence and conduction band offsets respectively (i.e., ~1eV narrower gap) [27].

ZrO_2

The photoemission and inverse photoemission data obtained from a 30 Å ZrO_2/SiO_xN_y/n-Si are shown in Figure 6. The valence band mainly consists of O 2p-like non-bonding orbitals of π-symmetry while the conduction band is mainly Zr 4d-like anti-bonding orbitals. The energy separations ΔE_{VBM} and ΔE_{CBM} are found to be 4.32 eV and 1.36 eV, respectively; consequently the band gap is extracted to be 5.68 eV. If, on the other hand, we take the conventional method of linear extrapolation of the valence and/or conduction band leading edge to the background intensity level, we obtain a value of 5.66 eV for the band gap. In this case, the straight line method yields a very similar result [28].

The theoretical density of states is convoluted with the instrumental response function, and is plotted along with the experimental measurement of valence and conduction bands (Figure 6). Good agreement is observed between the experimental and theoretical valence band density of states (specifically the band widths and edges), even though the transition matrix element argument indicated above is valid. In the case of the unoccupied conduction band, the width of the band and the band edge structures agree well with theory, although the intensity in the upper portion of the band is not in agreement. This discrepancy may result from differences in cross sections. This is somewhat expected since the atomic d-orbitals split due to the crystal field and have different symmetries. To a first approximation, assuming a cubic field around zirconium cations, the orbitals should split into doubly degenerate e_g and triply degenerate t_{2g}-orbitals. It should also be noted that the theoretical calculations are based on the ground state of the system; on the other hand, the measurement is inherently representative of excited states. We also note that our recent X-ray absorption studies on the L_2 and L_3 edges of ZrO_2 showed significant matrix element effects, which indicates different cross-sections for these orbitals [29].

The obtained valence and conduction band offsets (3.40 eV and 1.16 eV) are large enough to make ZrO_2 a viable candidate from a band alignment point of view. These values are in good agreement with those reported by Robertson [12,30]. However in order to be able to compare the values obtained, one would need to know the phase of the ZrO_2 reported in these studies. Having known the electron affinity of silicon and the conduction band offset, the "apparent" electron affinity of ZrO_2 can be extracted as 2.99 eV (Figure 5c).

Energy Band Parameter	Experiment / Theory (Perfect Crystal)		Effective values (Band-Tail Subtract)		Straight-line method	
	HfO_2	ZrO_2	HfO_2	ZrO_2	HfO_2	ZrO_2
Eg	6.70	5.68	5.84	-	5.86	5.66
EA	2.18	2.99	2.68	-	2.69	2.88
CBO	1.97	1.16	1.47	-	1.46	1.27
VBO	3.61	3.40	3.25	-	3.28	3.29

TABLE I. The extracted values for bandgap (E_g), electron affinity (EA), conduction band offset (CBO), valence band offset (VBO), and the energy separation between Hf $4f_{7/2}$ photo-electron line and valence band maximum (ΔE ($Hf4f_{7/2}$ - VBM)). Experiment/theory is determined by assuming perfect crystallinity while the effective values are extracted by including the band tail states (at the 2σ level). All values are in units of eV. The effective values for ZrO_2 are not shown since the comparison between theory and experiment did not reveal any observable intensity at the band edges.

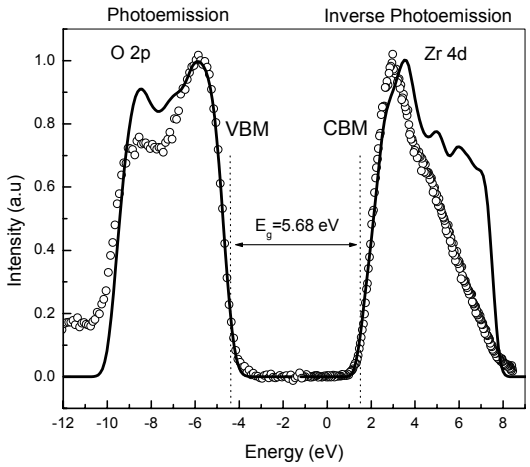

FIGURE 6. Combined photoemission and inverse photoemission spectra of a 30 Å ZrO_2/SiO_xN_y/n-Si gate stack along with convoluted DOS for amorphous ZrO_2.

Comparison of HfO_2 and ZrO_2 results: Band tail states

We have noted the "extra" density of states near the band edges observed for HfO_2 films. The theoretical calculations used to determine the band edges for HfO_2 are for monoclinic bulk oxide crystals of infinite extent (boundary conditions). Due to finite crystallinity of the ultrathin films and the presence of structural and compositional defects, electrical defects may appear, which are charged or neutral, according to their atomic nature, and could in principal exist anywhere (in space and/or energy) in the film. Experimentally, interfacial and/or bulk defect states are observed in a variety of alternative high permittivity materials, some with electrically measured defect densities on the order of 10^{13} $cm^{-2}{\cdot}eV^{-1}$. With good signal to noise, a near surface defect level of 5% might be observable by photoemission (although it is not clear what the relation is between the electrical and physical defect densities). Because of the observed excess density of states near the band edges and the consequence this has on the band edge definition, two values for the offsets as well as the bandgap are noted. One way to understand the defect state energies would be to assume a distribution of defect states in the vicinity of the band edges, as the data suggest. If the experimentally determined DOS is taken and subtracted from the theoretical DOS (following normalization), the difference yields two peaks close to the two band edges. These two peaks can be modeled as a pair of Gaussian curves (Figure 7) with centrums at -4.01 eV and 2.83 eV, and widths of 0.58 eV and 0.59 eV (after subtracting out the corresponding spectrometer response functions outlined above). The literature consensus is that HfO_2 films have a gap of 5.6 eV to 6.0 eV, although the proof and methodology of this remains debated [4,12,30-32]. We obtain this value from our results by defining the edge as the 2σ level of the Gaussian-modeled band tail states. Although there is no strong theoretical argument to include what we are calling band edge defect states in defining the "real" gap, they

may be considered as contributing to an "effective" band gap [27] (see Figure 7). We also include these effective values in Figure 5b.

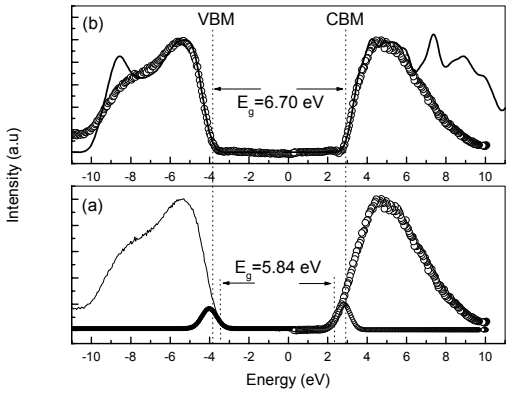

FIGURE 7. (a) Densities of states of monoclinic HfO_2 as determined by PES and IPES, the Gaussian peaks roughly model the presence of occupied and unoccupied band-tail/defect states in the vicinity of the VBM and CBM. (b) The fit between theoretical and experimental DOS improves after the band tail states subtracted from the measured DOS.

Concerning their physical nature, one of the conventional assignments of the observed defect states would be to attribute them to band-tail states. The presence of structural disorder can also be caused by (or related to) the deviations from ideal stoichiometry (metal vacancies, excess oxygen, oxygen vacancies, or impurities such as atomic hydrogen). In fact, these films do contain slightly higher oxygen content than the ideal stoichiometry (at least as measured by MEIS following growth) and are likely to contain excess hydrogen as deposited. Peacock and Robertson [31] have shown that atomic hydrogen, as an extrinsic defect, would introduce shallow unoccupied states in the vicinity of the conduction band which will behave as acceptors [33]. Foster et al. reported on the vacancy and interstitial defects in HfO_2 where it is theoretically shown that the O_2^- species would introduce defect states in the vicinity of the valence band. These states are neutral when occupied and act as donors [34].

We attributed the excess intensity in the band edges of HfO_2 to finite crystallinity of the ultrathin films (as evidenced by reduced crystallinity from XRD studies) and the presence of structural and compositional defects. However, in the case of ultrathin amorphous ZrO_2 studied here, the agreement between the experiment and the theory at the band edges is remarkable. Therefore, developing the correct theoretical model to describe these oxide phases and using the corresponding DOS to model the valence and conduction band is crucial not only for determining the band edge but also for developing an understanding of defect levels as exemplified here.

Spectroscopic Ellipsometry Results on ZrO_2 Ultrathin Films

Figure 8 presents the real (ε_1) and imaginary (ε_2) parts of dielectric functions of a series of thin ZrO_2 films. The dependence on thickness and thermal annealing are the two important trends observed in the dielectric functions. As the thickness of as-deposited films increased above a transitional value, somewhere between 54 Å and 64 Å, the optical bandgap (determined by Tauc plots) increased from 5.1 eV to 5.5 eV and remained at 5.5 eV for thicker films. Uncertainty of band-gap values derived from the Tauc plots is estimated to be about 0.05 eV. In addition, the dielectric function exhibits new interband transitions (≈ 6.0 eV, 7.3 eV, and 8.5 eV), and the overall magnitude increases with thickness. The same interband transitions and increase in the bandgap of the thin samples is observed after thermal anneals at various ambients.

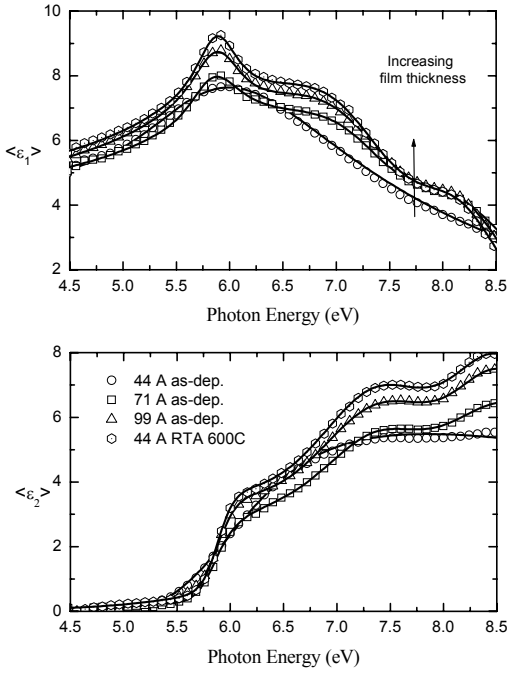

FIGURE 8. Dielectric functions of ZrO_2 films resulting from VUV spectroscopic ellipsometry for as-deposited films of 44, 71, and 99 Å and for a 53 Å film after RTA 600 °C. Real (top) and imaginary (bottom) parts of dielectric functions.

Concluding Remarks

As a note of caution, we point out that semiconductor energy gaps are specific to the method(s) used to determine them. It is important to note that photoemission and inverse photoemission give a one particle energy gap that, although wider than the conventionally reported optical gap (usually involving an exciton), may be more relevant to understanding tunneling through a dielectric. Other methods of gap and edge determination such as spectroscopic ellipsometry (SE), UV/VIS spectroscopy, XPS "shake up" spectral analysis, near-edge XAS, include the exciton energy which may be as high as 1 eV to 2 eV in some oxides.

Combined PES and IPES studies, here, revealed a bandgap of 5.68 eV for ZrO_2 whereas the ellipsometric optical bandgap for the same sample indicates a bandgap of 5.1 eV. The difference in the bandgap values (~0.6 eV) can be attributed to the final state effects of the relevant excitations. In the case of PES measurements, the final state is a hole in the valence band; in that of IPES, the final state consists of an extra electron in the conduction band. In the ellipsometry case, the final state is a hole in valence band and an electron in the conduction band, where an exitonic effect may be contributing to the observed bandgap when compared to the PES-IPES determined one. This comparison, of course, is valid with the assumption that the band edge determination errors are comparable.

These findings lead one to consider several important issues when thinking of dielectric design and metrology:

(i) Since the tetragonal phase has a larger dielectric constant ($\varepsilon \approx 35$) than amorphous, monoclinic, or cubic ZrO_2, it may be desirable to stabilize the tetragonal ZrO_2 phase for gate dielectric applications (assuming that it can be made homogeneous across the gate regions). This may be achieved by tailoring film thickness or annealing the gate stack (if the film is in a metastable state), both of which can lead to formation of the tetragonal phase. Another route is to stabilize a certain phase by impurity incorporation, as is often done for the cubic phase. By growing under conditions which prefer (or stabilize) the tetragonal phase, one can take advantage of higher dielectric constant (lower equivalent oxide thickness - EOT), larger bandgap, and lower leakage. Unfortunately, there will be a trade-off in the case of gate stack design. Our results imply that if the film is too thin, then the film may exhibit only an amorphous phase, whereas for intermediate thickness films (>5 nm), the more-stable tetragonal phase is able to form. A thermodynamic rationale for the observed thickness dependent phase evolution is given in reference 35. An alternative kinetic rationalization is that (a) the time-at-temperature is directly related to deposited film thickness, and/or (b) a greater number of nucleation sites may exist in thicker metal oxide films. HfO_2 and other high-κ dielectric materials systems may have similar properties.

(ii) The change of crystal structure will also have important consequences from a band alignment point of view. The tetragonal phase has a larger bandgap than the amorphous phase by about ≈ 0.4 eV (Figure 8) [14]. This will lead to different band offsets and thereby affect charge transport and leakage current. A small change in barrier height (e.g., 0.1 eV) can affect the leakage current appreciably.

(iii) From a metrology point of view, effects of phase on the dielectric properties (e.g., dielectric function) must be fully understood for any given system. Using the conventional approach to determine dielectric constant (optical thickness vs EOT) will be inaccurate if the thickness regime results in multiple crystalline phases. Phase changes that are beneficial from a dielectric constant perspective may have a negative effect on mobility since the relatively high dielectric constant for this class of materials is a result of low frequency soft-phonon contributions which in turn is though to contribute to electron scattering in the channel.

Summary

We have applied several important spectroscopic techniques to characterize the material phase and electronic structure of two prominent high-κ gate dielectric candidate materials to elucidate the energy band barrier heights, band-gaps, and band-offsets. As a result of these extensive characterization efforts, we have shown that both of these materials are viable high-κ candidates from a barrier height perspective. We have demonstrated the effect of crystal phase on the electronic and dielectric properties of these materials including energies and the origin of defect levels and discussed important possible implications and consequences of these interactions and dependencies.

Acknowledgements

Figures and discussions presented in parts of this review have appeared in some of our earlier publications noted in the text. The authors would like to acknowledge the financial support of SRC, SEMATECH, NSF, and the NIST Office of Microelectronic Programs.

REFERENCES

1. ITRS, International Technology Roadmap for Semiconductors, 2003 Edition). Semiconductor Industry Association, Available from International SEMATECH, Austin TX
2. G. D. Wilk, R. M. Wallace, and J. M. Anthony, J. Appl. Phys. **89,** 5243 (2001).
3. I. Barin and O. Knacke, *Thermodynamic Properties of Elements and Oxides* (Springer-Verlag, Berlin, 1973).
4. M. Balog, M. Schieber, M. Michman, and S. Patai, Thin Solid Films **41,** 247-259 (1977).
5. C. T. Hsu, Y. K. Su, and M. Yokoyama, Jpn. J. Appl. Phys. **31,** 2501 (1992).
6. S. J. Lee, H. F. Luan, W. P. Bai, C. H. Lee, T. S. Jeon, Y. Senzaki, D. Roberts, and D. L. Kwong, Electron Devices Meeting, 2000, IEDM Technical Digest, IEEE, New York, N.Y. pp 2.4.1-2.4.4
7. Y.-S. Lin, R. Puthenkovilakam, and J. P. Chang, Appl. Phys. Lett. **81,** 2041-2043 (2002).
8. M. Balog, M. Schieber, M. Michman, and S. Patai, Thin Solid Films **47,** 109-120 (1977).
9. B.-O. Cho, J. Wang, L. Sha, and J. P. Chang, Appl. Phys. Lett. **80,** 1052-1054 (2002).
10. M. Houssa, V. V. Afanas'ev, and A. Stesmans, Appl. Phys. Lett. **77,** 1885-1887 (2000).
11. S. Ramanathan, P. C. McIntyre, J. Luning, P. Pianetta, and D. A. Muller, Phil. Mag. Lett. **82,** 519-528 (2002).
12. J. Robertson, J. Vac. Sci. Tech. B **18,** 1785-1791 (2000).
13. S. Sayan, M. Croft, N. V. Nguyen, T. Emge, E. Gusev, H. Kim, J. Ehrstein, P. J. McIntyre, and E. Garfunkel, Appl. Phys. Lett. **86,** 152902 (2005).
14. X. Zhao and D. Vanderbilt, Mat. Res. Soc.Symp. Proc. Vol. **745,** Fall Meeting 2002, Materials Research Society, Pittsburgh, PA, pp. 93-98 (2003).
15. X. Zhao and D. Vanderbilt, Phys. Rev. B **65,** 233106/1-4 (2002).
16. X. Zhao and D. Vanderbilt, Phys. Rev. B **65,** 075105/1-10 (2002).
17. D. Redfield, J. P. Wittke, and J. I. Pankove, Phys. Rev. B **2,** 1830-1839 (1970).
18. C. H. Olk and S. M. Yalisove, Phys. Rev. B **52,** 1692-1697 (1995).
19. P. Y. Yu and M. Cardona, in *Fundamentals of Semiconductors*, Third ed. (Springer-Verlag Berlin Heidelberg, New York, 2001), p. 159-202.
20. S. Sayan, S. Aravamudhan, B. W. Busch, W. H. Schulte, F. Cosandey, G.D.Wilk, T. Gustafsson, and E. Garfunkel, J. Vac. Sci. Tech. A **20,** 507-512 (2002).
21. M. A. Gribelyuk, A. Callegari, E. P. Gusev, M. Copel, and D. A. Buchanan, J. Appl. Phys. **92,** 1232-1237 (2002).
22. Y. Jeon, J. Chen, and M. Croft, Phys. Rev. B **50,** 6555-6563 (1994).
23. F. M. F. d. Groot, Physica B **208-209,** 15-18 (1995).
24. D. Vanderbilt, X. Zhao, and D. Ceresoli, Proceedings of the 11th International Workshop on Oxide Electronics, Hakone, Japan, October 2004; Thin Solid Films **(in press)** (2005).
25. S. M. Sze, *Physics of Semiconductor Devices*, Second ed. (John Wiley & Sons, New York, 1981).
26. K. Kano, *Semiconductor Devices* (Prentice-Hall Inc., Upper Saddle River, NJ, 1998).
27. S. Sayan, E. Garfunkel, R. A. Bartynski, S. Suzer, and M. Banaszak Holl, J. Appl. Phys. **96,** 7485-7491 (2004).
28. S. Sayan, R. A. Bartynski, X. Zhao, E. P. Gusev, E. Garfunkel, D. Vanderbilt, M. Croft, S. Suzer, and M. B. Holl, Phys. Stat. Sol. B **241,** 2246-2252 (2004).
29. D. Vanderbilt, Phys. Rev. B **41,** 7892-7895 (1990).
30. J. Robertson, Appl. Surf. Sci. **190,** 2-10 (2002).
31. V. V. Afanas'ev, A. Stesmans, F. Chen, X. Shi, and S. A. Campbell, Appl. Phys. Lett. **81,** 1053-1055 (2002).
32. A. Callegari, E. Cartier, M. Gribelyuk, H. F. Okorn-Schmidt, and T. Zabel, J. Appl. Phys. **90,** 6466-6475 (2001).
33. P. W. Peacock and J. Robertson, Appl. Phys. Lett. **83,** 2025-2027 (2003).
34. A. S. Foster, F. L. Gejo, A. L. Shluger, and R. M. Nieminen, Phys. Rev. B **65,** 174117 (2002).
35. S. V. Ushakov, C. E. Brown, A. Navrotsky, A. Demkov, C.Wang, and B.-Y. Nguyen, Mat. Res. Soc. Symp. Proc. Vol. 745; Fall Meeting 2002; Materials Research Society, Pittsburgh PA pp. 3-8, (2003).